Bridging 3D Anomaly Localization and Repair via High-Quality Continuous Geometric Representation

Supplementary Material

A. Data Preparation Details

Our pipeline processes raw 3D meshes into signed distance function (SDF) training samples through geometric normalization and multi-scale sampling. During training, each input mesh undergoes coordinate normalization to align all axes within the $[0,1]^3$ domain. We validate geometric integrity using a hybrid watertightness check: First, we detect non-manifold edges through topological analysis of the face adjacency graph. Meshes failing this check are processed through Poisson surface reconstruction to generate watertight counterparts.

Query points are sampled through a multi-scale strategy: **(1) global volume sampling** across the normalized $[0,1]^3$ domain generates global context points, **(2) adaptive bounding box sampling** operates within a 1.3× expanded object-aligned bounding box to concentrate queries in surface-proximal regions, and **(3) surface-constrained sampling** employs barycentric coordinate interpolation on mesh faces, prioritizing high-curvature regions through triangle area-weighted selection to densely encode the SDF zero-crossing manifold. The signed distance value for a query point $\boldsymbol{x}$ is:

$$\text{SDF}(\boldsymbol{x}) = \|\boldsymbol{x} - \boldsymbol{p}_s\|_2 \cdot \text{sgn}\big(\boldsymbol{n}_s^\top (\boldsymbol{x} - \boldsymbol{p}_s)\big) \tag{1}$$

where $\boldsymbol{p}_s$ is the nearest surface point to $\boldsymbol{x}$ (retrieved via KD-tree acceleration), $\|\boldsymbol{x} - \boldsymbol{p}_s\|_2$ is the absolute distance from $\boldsymbol{x}$ to the surface, $\boldsymbol{n}_s$ denotes the outward-oriented unit normal at $\boldsymbol{p}_s$, and $\text{sgn}(\cdot)$ enforces the geometric sign convention:

$$\text{sgn}(v) = \begin{cases} -1 & \text{if } v < 0 \quad (\textit{inside}) \\ +1 & \text{otherwise} \quad (\textit{outside}). \end{cases} \tag{2}$$

The sign assignment follows a consistent logic: points located inside the shape reside in the negative half-space defined by the surface normal, satisfying $\boldsymbol{n}_s^\top (\boldsymbol{x} - \boldsymbol{p}_s) < 0$, while those in the positive half-space are classified as outside. This approach ensures alignment with the assumption that the mesh is watertight. Furthermore, it is well-suited for point cloud representations that include internal structures, as the explicit separation of distance and sign enables robust handling of enclosed cavities and nested surfaces, ensuring accurate SDF computation even in complex, multi-layered geometries.

B. Evaluation Metrics for Anomaly Repair

To quantitatively evaluate 3D anomaly repair, we use Chamfer Distance and Earth Mover's Distance, which assess geometric accuracy and structural consistency.

Chamfer Distance (CD). Chamfer Distance measures the discrepancy between two point sets by computing the sum of squared distances from each point to its nearest neighbor in the other set. Given a reconstructed shape S_1 and the ground truth S_2, it is defined as:

$$d_{\text{CD}}(S_1, S_2) = \sum_{x \in S_1} \min_{y \in S_2} \|x - y\|_2^2 + \sum_{y \in S_2} \min_{x \in S_1} \|x - y\|_2^2. \tag{3}$$

Here, $x \in S_1$ and $y \in S_2$ are points in the reconstructed and ground truth point sets, respectively, and $\|\cdot\|_2$ denotes the Euclidean distance. CD efficiently captures point-wise accuracy, making it suitable for evaluating local geometric deviations. However, it does not impose a structured mapping between the distributions of S_1 and S_2, potentially leading to misalignment in cases where shapes exhibit global structural shifts.

Earth Mover's Distance (EMD). Earth Mover's Distance, also known as the Wasserstein distance, measures the minimum transport cost required to transform one point set into another. Unlike CD, which only considers nearest neighbors, EMD enforces a one-to-one correspondence by finding an optimal bijection $\phi : S_1 \to S_2$:

$$d_{\text{EMD}}(S_1, S_2) = \min_{\phi: S_1 \to S_2} \sum_{x \in S_1} \|x - \phi(x)\|_2. \tag{4}$$

In this formulation, $\phi(x)$ represents the optimal match for each x in the ground truth set S_2, ensuring that mass transport is minimized. EMD provides a more global assessment of structural consistency, penalizing uneven distributions that Chamfer Distance might overlook. Due to its higher computational complexity, it is typically computed on a subset of points.

C. More Qualitative Results

Due to page limit, only a limited number of qualitative results are presented in the main text. To offer a more comprehensive and intuitive visualization of our results, we provide additional qualitative results in Figure A, B. Specifically, the first column displays the original surface, the second column shows the anomaly map, and the third column presents the repaired surface.

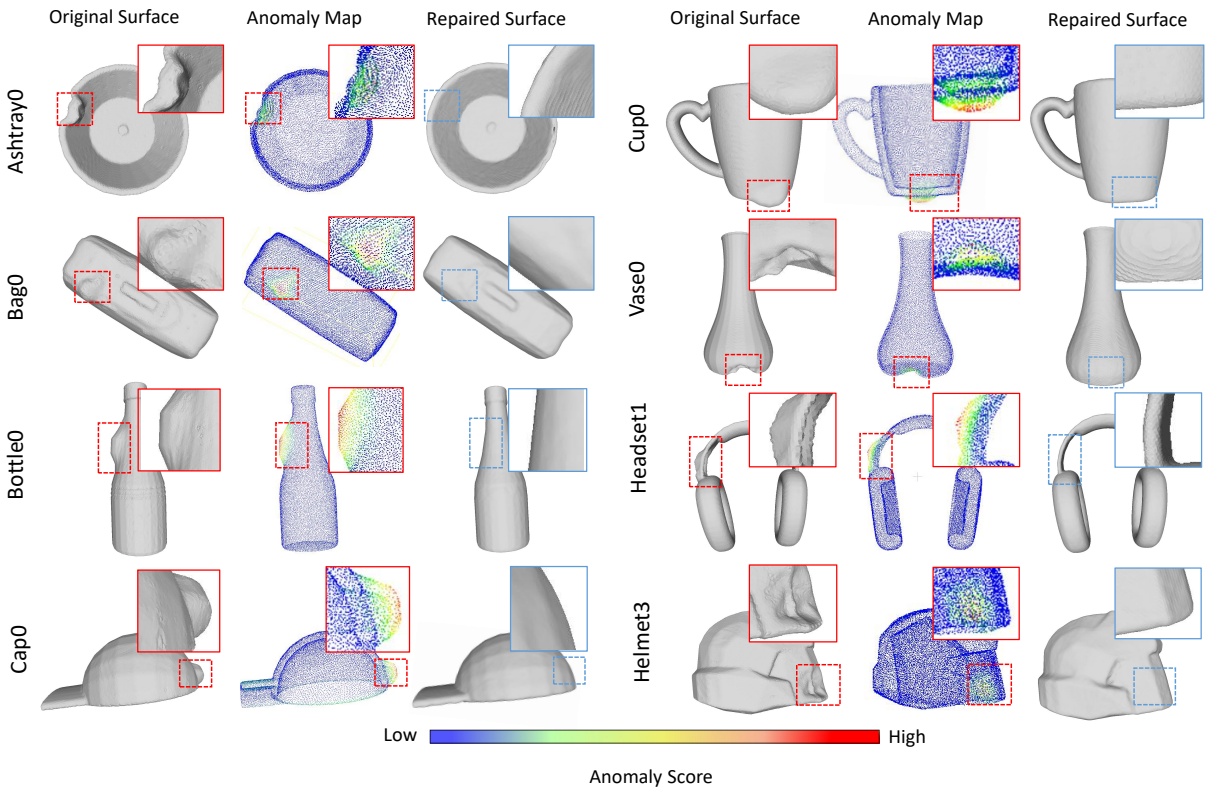

Figure A. Qualitative anomaly localization results on Anomaly-ShapeNet.

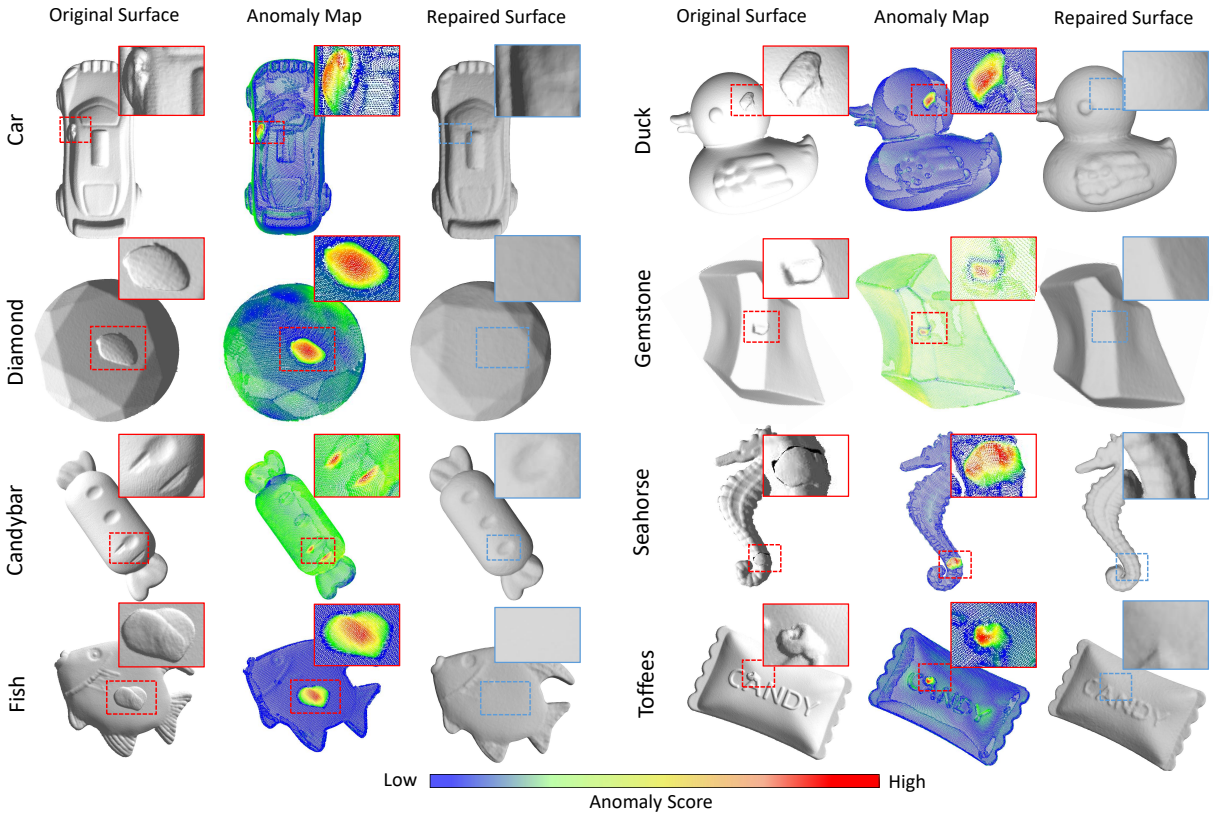

Figure B. Qualitative anomaly localization results on Real3D-AD.

Method	cap0	cap3	helmet3	cup0	bowl4	vase3	headset1	eraser0	vase8	cap4	vase2	vase4	helmet0	bucket1	vase7	helmet2	cap5	shelf0	bowl5	bowl3	helmet1
BTF(FPFH)	0.618	0.522	0.444	0.586	0.609	0.699	0.490	0.719	0.668	0.520	0.546	0.510	0.571	0.633	0.518	0.542	0.586	0.609	0.699	0.490	0.719
BTF(FPFH) with PAM	0.741	0.740	0.567	0.881	0.644	0.433	0.680	0.810	0.558	0.533	0.652	0.609	0.635	0.444	0.629	0.684	0.653	0.530	0.632	0.786	0.648
Patchcore(FPFH)	0.580	0.453	0.404	0.600	0.494	0.449	0.637	0.657	0.662	**0.757**	0.721	0.506	0.546	0.551	0.693	0.425	0.790	0.494	0.558	0.537	0.484
Patchcore(FPFH) with PAM	**0.996**	**0.811**	0.624	0.914	0.863	0.679	0.781	**1.000**	0.852	0.744	**1.000**	0.848	0.432	0.603	0.881	**0.788**	0.800	**0.786**	0.828	0.644	0.729
Patchcore(PointMAE)	0.589	0.476	0.424	0.610	0.501	0.460	0.627	0.677	0.663	0.727	0.741	0.516	0.556	0.561	0.650	0.447	0.538	0.523	0.593	0.579	0.552
Patchcore(PointMAE) with PAM	0.619	0.660	0.455	0.605	0.385	0.664	0.462	0.790	0.694	0.407	0.614	0.542	0.441	**0.832**	0.600	0.609	0.744	0.580	0.554	0.470	0.338
PASDF(Ours)	0.852	0.649	**0.846**	**0.971**	**0.933**	**0.806**	**0.795**	0.952	**0.924**	0.646	**1.000**	**0.912**	**0.812**	0.775	**1.000**	0.765	**0.853**	0.713	**0.912**	**1.000**	**0.938**

Method	bottle3	vase0	bottle0	tap1	bowl0	bucket0	vase5	vase1	vase9	ashtray0	bottle1	tap0	phone	cup1	bowl1	headset0	bag0	bowl2	jar0	**Mean**
BTF(FPFH)	0.322	0.342	0.344	0.546	0.509	0.401	0.409	0.219	0.268	0.420	0.546	0.560	0.671	0.610	0.668	0.520	0.546	0.510	0.424	0.528
BTF(FPFH) with PAM	0.822	0.779	0.705	0.533	0.833	0.724	0.495	0.457	0.612	0.686	0.523	0.661	0.676	0.552	0.552	0.693	0.714	0.559	0.295	0.579
Patchcore(FPFH)	0.572	0.455	0.604	0.766	0.504	0.469	0.417	0.423	0.660	0.587	0.667	0.753	0.388	0.586	0.639	0.583	0.571	0.615	0.472	0.568
Patchcore(FPFH) with PAM	0.990	0.925	0.962	0.507	0.974	**0.981**	0.752	0.767	**0.882**	0.919	0.951	0.691	**1.000**	0.771	0.819	0.942	0.710	0.407	**1.000**	0.814
Patchcore(PointMAE)	0.650	0.447	0.513	0.538	0.523	0.593	0.579	0.552	0.629	0.591	0.601	0.458	0.488	0.556	0.629	0.591	0.601	0.458	0.483	0.562
Patchcore(PointMAE) with PAM	0.517	0.887	0.652	0.537	0.641	0.559	0.657	0.443	0.564	0.781	0.779	0.736	0.710	0.481	0.522	0.707	0.538	0.563	0.738	0.627
PASDF(Ours)	**1.000**	**1.000**	**1.000**	**0.793**	**1.000**	0.968	**1.000**	**0.929**	0.836	**1.000**	**1.000**	**0.882**	**1.000**	**0.857**	**0.948**	**1.000**	**0.995**	**1.000**	**1.000**	**0.900**

Table A. O-AUROC score (↑) on Anomaly-ShapeNet dataset. The best and second-best results are marked in **bold** and underlined.

Method	cap0	cap3	helmet3	cup0	bowl4	vase3	headset1	eraser0	vase8	cap4	vase2	vase4	helmet0	bucket1	vase7	helmet2	cap5	shelf0	bowl5	bowl3	helmet1
BTF(FPFH)	0.730	0.658	0.724	0.790	0.679	0.699	0.591	0.719	0.662	0.524	0.646	0.710	0.575	0.633	0.540	0.643	0.586	0.619	0.699	0.690	**0.749**
BTF(FPFH) with PAM	0.864	0.699	0.608	0.892	0.611	0.568	0.505	0.894	0.586	0.689	0.872	0.650	0.731	0.648	0.682	0.524	0.803	0.769	0.715	0.807	0.533
Patchcore(FPFH)	0.472	0.653	0.737	0.655	0.720	0.430	0.464	0.810	0.575	0.595	0.721	0.505	0.548	0.571	0.693	0.455	0.795	0.613	0.358	0.327	0.489
Patchcore(FPFH) with PAM	**0.973**	**0.921**	0.856	**0.976**	0.860	0.752	0.850	**0.946**	0.856	**0.966**	**0.978**	**0.964**	0.806	0.783	0.958	**0.818**	**0.958**	**0.883**	0.774	**0.972**	0.732
Patchcore(PointMAE)	0.544	0.488	0.615	0.510	0.501	0.465	0.423	0.378	0.364	0.725	0.742	0.523	0.580	0.754	0.651	0.651	0.545	0.543	0.562	0.581	0.562
Patchcore(PointMAE) with PAM	0.739	0.752	0.660	0.663	0.436	0.601	0.605	0.626	0.680	0.702	0.691	0.748	0.569	**0.880**	0.568	0.642	0.802	0.687	0.528	0.586	0.572
PASDF(Ours)	0.948	0.861	**0.958**	0.948	**0.865**	**0.868**	**0.891**	0.945	**0.909**	0.894	0.956	0.899	**0.816**	0.824	**0.959**	0.809	0.920	0.865	**0.909**	0.939	0.646

Method	bottle3	vase0	bottle0	tap1	bowl0	bucket0	vase5	vase1	vase9	ashtray0	bottle1	tap0	phone	cup1	bowl1	headset0	bag0	bowl2	jar0	**Mean**
BTF(FPFH)	0.622	0.642	0.641	0.596	0.710	0.401	0.429	0.619	0.568	0.624	0.549	0.568	0.675	0.619	0.768	0.620	0.746	0.518	0.427	0.628
BTF(FPFH) with PAM	0.809	0.837	0.880	0.674	0.769	0.772	0.567	0.652	0.695	0.693	0.696	0.647	0.869	0.687	0.548	0.717	0.841	0.621	0.852	0.683
Patchcore(FPFH)	0.512	0.655	0.654	0.768	0.524	0.459	0.447	0.453	0.663	0.597	0.687	0.733	0.488	0.596	0.531	0.583	0.574	0.625	0.478	0.580
Patchcore(FPFH) with PAM	0.889	0.929	**0.985**	0.716	**0.981**	0.842	0.713	0.757	**0.905**	0.774	0.841	0.827	0.943	0.758	0.732	0.807	0.895	0.814	**0.985**	0.867
Patchcore(PointMAE)	0.653	0.677	0.553	0.541	0.527	0.586	0.572	0.551	0.423	0.495	0.606	0.858	0.886	0.856	0.524	0.575	0.674	0.515	0.487	0.577
Patchcore(PointMAE) with PAM	0.883	0.835	0.691	0.681	0.656	0.574	0.602	0.675	0.719	0.765	0.735	0.687	0.792	0.569	0.566	0.646	0.593	0.525	0.774	0.681
PASDF(Ours)	**0.948**	**0.944**	0.951	**0.902**	0.963	**0.875**	**0.915**	**0.797**	0.863	**0.919**	**0.926**	**0.884**	**0.951**	**0.884**	**0.900**	**0.863**	**0.958**	**0.816**	0.959	**0.897**

Table B. P-AUROC score (↑) on Anomaly-ShapeNet dataset. The best and second-best results are marked in **bold** and underlined.

Method	**O-AUROC ↑**	**P-AUROC ↑**
w/o RANSAC	0.550	0.570
w/o ICP	0.712	0.667
w/o IO	0.781	0.738
w/o PE	0.750	0.706
PASDF (Full)	**0.802**	**0.745**

Table C. Ablation study on Real3D-AD. IO represents iterative optimization. PE stands for positional encoding.

D. Detailed Results of Ablation Studies

In the main text (Table 5), we present the overall results of the PAM ablation study, demonstrating its effectiveness in improving anomaly detection performance across different baseline models on Anomaly-ShapeNet. To provide a more detailed analysis, we report the per-class quantitative results in Table A, B. These results offer a finer-grained evaluation of PAM's impact on individual object categories, further validating its robustness and generalization ability.

In the main text (Table 6), we provide ablation experiments for PAM on Anomaly-Shapenet dataset. Additionally, in Table C we supplement the ablation experiments on Real3D-AD. PAM consistently improves the baselines, and its components are crucial for PASDF on Real3D-AD, demonstrating generalizability.

E. Comparative discussion with PO3AD

Recent work PO3AD [1] detect anomalies through point offset predictions similar to our use of Signed Distance Fields (SDFs). However, unlike our method, PO3AD relies on synthetic pseudo-anomalies and does not address pose alignment or anomaly repair.

References

[1] Jianan Ye, Weiguang Zhao, Xi Yang, Guangliang Cheng, and Kaizhu Huang. Po3ad: Predicting point offsets toward better 3d point cloud anomaly detection. In *Proceedings of the Computer Vision and Pattern Recognition Conference*, pages 1353–1362, 2025. 3